Journal of Zhejiang University-SCIENCE A (Applied Physics & Engineering) 2025 26(7):666-678
www.jzus.zju.edu.cn; www.springer.com/journal/11582
E-mail: jzus_a@zju.edu.cn

Research Article

https://doi.org/10.1631/jzus.A2400405

Check for updates

Flow loss characteristics in parallel confluence sections of tunnels

Xin ZHANG[1], Hao HE[1], Xiaofeng CHEN[2,3], Yachao LI[4], Tianhang ZHANG[2,3,6]✉, Yuehui WANG[4], Kai ZHU[5], Ke WU[2,3]✉

[1]*School of Electronic Engineering, Xi'an Shiyou University, Xi'an 710065, China*
[2]*Center for Balance Architecture, Zhejiang University, Hangzhou 310028, China*
[3]*Research Center for Urban Fire Safety Engineering, Zhejiang University, Hangzhou 310058, China*
[4]*China Railway Tunnel Stock Co., Ltd., Zhengzhou 450007, China*
[5]*College of Energy Environment and Safety Engineering, China Jiliang University, Hangzhou 310018, China*
[6]*Research Center for Smart Urban Resilience and Firefighting, The Hong Kong Polytechnic University, Hong Kong 999077, China*

Abstract: The construction of bifurcated tunnels is essential to advancing urban infrastructure systems, as they conserve land, reduce carbon emissions, and optimize traffic. However, the bifurcation structure of the parallel confluence section of such tunnels poses significant challenges in the design and operation of the tunnel ventilation system, in terms of both the internal and external environment. In this work, the flow and loss characteristics of parallel confluence sections are studied with numerical simulations and model experiments. The influences of the confluence ratio q and the confluence angle θ on the flow characteristics and loss mechanisms of the parallel confluence section are revealed theoretically. The results indicate that when q is small, the high-velocity airflow from the mainline entrains the low-speed airflow from the ramp, leading to flow separation at the upper connection between the parallel section and the gradual transition section; when q is large, the high-velocity airflow from the ramp entrains the low-speed airflow from the mainline, resulting in flow separation on the side of the confluence section adjacent to the mainline. Additionally, the mismatch between the airflow ratio Q and cross-sectional area ratio φ of the mainline tunnel and the ramp prior to confluence enhances the jet entrainment effect, increases the curvature of the streamline, expands the range of the flow separation area, and generates higher confluence loss coefficients $|K_{13}|$ and $|K_{23}|$ of the mainline and the ramp. For small q, K_{13} and K_{23} remain relatively constant with respect to θ, whereas for large q, both $|K_{13}|$ and $|K_{23}|$ decrease as θ increases. Finally, a semi-empirical formula is proposed to predict the loss coefficients for parallel bifurcated tunnels with confluence angles ranging from 5° to 15°. This study provides insights into the aerodynamic behaviour and loss mechanisms in bifurcated tunnels, offering guidelines for enhancing the efficiency of tunnel ventilation systems in tunnel-like underground infrastructure.

Key words: Parallel bifurcated tunnel; Confluence ratio; Flow characteristics; Loss coefficients

1 Introduction

Urban highway tunnels play a crucial role in alleviating traffic congestion and shortening travel distances (Liang et al., 2021; Gao et al., 2024; Zhang et al., 2024). These tunnels often feature inlet and exit ramps to connect surface roads and cater to traffic flow in key areas, like central business districts and transport hubs (Król and Król, 2021; Xu et al., 2022; Wang et al., 2024). The presence of inlet ramps leads to a confluence effect, which alters air and pollutant distribution within the tunnel and impacts its internal and external environment. This confluence also increases local resistance, reduces jet fan efficiency, and hampers fire and smoke control as compared to linear tunnels (Chen et al., 2021; Jafari et al., 2023). Therefore, understanding the flow and loss characteristics in these confluence sections is essential for designing energy-efficient ventilation systems and effective smoke control measures in bifurcated tunnels.

Confluence tunnels share structural similarities with confluence ducts, and extensive research has been conducted on the loss characteristics of these ducts.

✉ Tianhang ZHANG, tianhang.zhang@connect.polyu.hk
Ke WU, wuke@zju.edu.cn
Xin ZHANG, https://orcid.org/0000-0002-1613-7082
Tianhang ZHANG, https://orcid.org/0000-0002-8806-4492
Ke WU, https://orcid.org/0000-0003-2313-3124

Received Aug. 19, 2024; Revision accepted Oct. 20, 2024;
Crosschecked Apr. 23, 2025; Online first June 18, 2025

Studies have shown that in confluence pipes with an included angle ranging from 90° to 150°, fluids from the main and branch pipes converge at the bifurcation, contracting first and then expanding, resulting in local confluence losses (Li et al., 2001). The local loss coefficient at the confluence is influenced by variables such as the confluence ratio, cross-sectional area ratio, and confluence angle. Researchers (Blaisdell and Manson, 1963; Miller, 1971; Itō and Imai, 1973; Abou-Haidar and Dixon, 1992) have conducted experiments to determine the local loss coefficient within a confluence angle range of 45° to 120°, examining how it varies with flow rate ratio, cross-sectional area ratio, and confluence angle. Gardel (1957) developed an empirical formula to effectively predict the local loss coefficient based on model test data, while Oka et al. (1996) and Bassett et al. (2001) derived theoretical formulas for the local loss coefficient at confluence angles between 45° and 120°, based on the conservation theorem. However, in practical tunnel engineering the confluence angle is typically less than 30°; this is in order to avoid abrupt changes in travel direction when traffic from inlet ramps merges into the mainline and to enhance the safety and comfort of drivers and passengers (Zhang et al., 2018, 2019). Liu et al. (2020) used computational fluid dynamics (CFD) simulations to study the Biaoshuiyan Underground Interchange Tunnel of the Huaping to Lijiang Expressway, China. They focused on the effects of confluence angles between 10° and 30° on ventilation characteristics for a confluence ratio (the ratio of the airflow on the ramp to that on the mainline after confluence) of 0.5. Their results showed that larger confluence angles significantly increase the phenomenon of ramp backflow. It is important to note that in actual tunnels, the flows of traffic on the mainline and ramps are complex, and the confluence ratio is not constant; this therefore limits the applicability of findings from a single confluence ratio on real-world tunnel ventilation design. Chen et al. (2024) combined CFD simulations with scale model testing to further analyze the impact of confluence ratios (0.1–0.9) and angles (5°–15°) on the local loss coefficient of confluence. They proposed a semi-empirical formula based on Bassett's formula to accurately predict the local loss coefficient for tunnels with confluence angles of 5° to 15°.

It should be noted that to meet the requirements for vehicles to adjust their speed at tunnel bifurcations (such as decelerating before entering the exit ramp from the mainline and accelerating after merging into the mainline from the entrance ramp), an additional lane, referred to as a speed-change lane, is typically established between the mainline and the ramp. This lane allows for variable speed adjustments, diversions, and merging operations. Speed-change lanes are generally classified into two types: direct and parallel. The parallel speed-change lane is comprised of two components: a parallel section and a gradual transition section, with the parallel section being an additional lane added alongside the mainline, as illustrated in Fig. 1a. In contrast, the direct speed-change lane includes only the gradual transition section and no parallel section (Fig. 1b). Consequently, tunnel bifurcations can be categorized into two forms: direct bifurcation and parallel bifurcation. Currently, research on the characteristics of confluence losses in tunnels has primarily focused on direct bifurcations, with limited attention being given to the confluence resistance characteristics of parallel bifurcations. However, in parallel bifurcations, both the parallel section and the gradual transition section affect the formation of flow separation, thereby complicating the flow characteristics and loss mechanisms in the confluence section. Zhu et al. (2024) utilized a scaled experimental platform for bifurcation tunnels as well as CFD simulations to compare the characteristics of dividing flow into parallel and direct bifurcations with an angle of 0°. They discovered that compared to direct bifurcations, parallel bifurcations have a lower local resistance coefficient for the ramp and a higher local resistance coefficient for the mainline when the diversion ratio is small, while the opposite is true for a larger diversion ratio. Thus, the research findings regarding the local loss coefficients for direct bifurcations cannot be directly applied to parallel bifurcations.

This study employs CFD to develop a 3D mathematical model that simulates airflow in parallel confluence tunnels. By combining numerical simulations and scaled model experiments, we analyze the flow characteristics of the parallel confluence section and the variations of the loss coefficient with respect to the confluence ratio and angle. A semi-empirical theoretical formula for the confluence loss coefficient is established for design purposes. The results provide a theoretical foundation for predicting the confluence loss coefficient in parallel bifurcation tunnels.

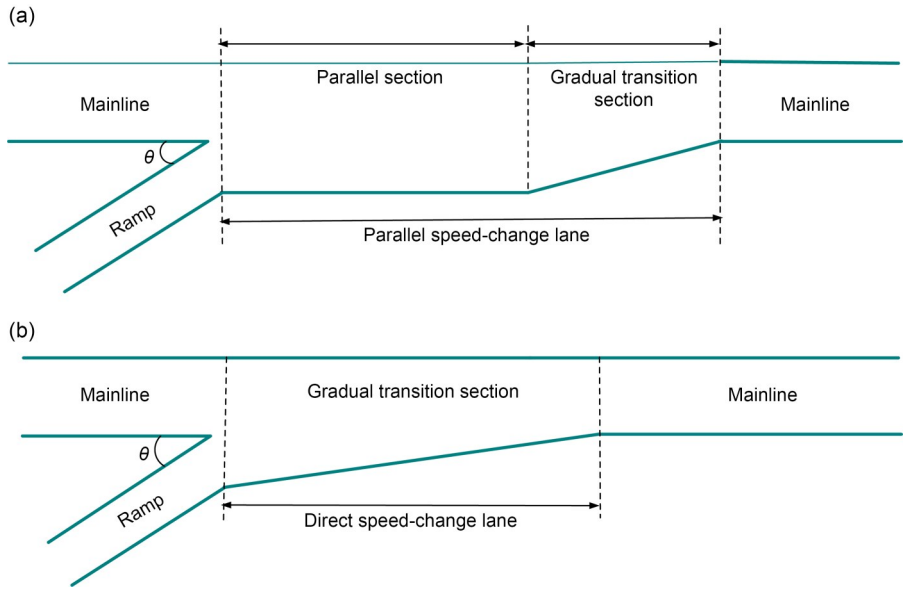

Fig. 1 Schematic diagrams of two types of tunnel bifurcations: (a) parallel bifurcation; (b) direct bifurcation

2 Mathematical modeling

2.1 Control equation and solution methods

We use the realizable k-ε turbulence model (Shih et al., 1995a), which demonstrates high prediction accuracy for phenomena such as boundary layer separation, streamline bending, reflux, and rotation with large counterpressure gradients, to calculate the air motion in a parallel confluence tunnel. Assuming that the airflow inside the tunnel is incompressible with constant values of viscosity and density (so the turbulent kinetic energy generation term caused by buoyancy and the expansion dissipation term caused by compressibility can be neglected), the turbulent kinetic energy k and turbulent kinetic energy dissipation rate ε transport equations are as follows:

$$\frac{\partial(\rho k)}{\partial t}+\frac{\partial(\rho k u_i)}{\partial x_i}=\frac{\partial}{\partial x_j}\left[\left(\mu+\frac{\mu_t}{\sigma_k}\right)\frac{\partial k}{\partial x_j}\right]+G_k-\rho\varepsilon, \quad (1)$$

$$\frac{\partial(\rho\varepsilon u_i)}{\partial x_i}=\frac{\partial}{\partial x_j}\left[\left(\mu+\frac{\mu_t}{\sigma_\varepsilon}\right)\frac{\partial \varepsilon}{\partial x_j}\right]+\rho C_1 S\varepsilon-\rho C_2\frac{\varepsilon^2}{k+\sqrt{\nu\varepsilon}}, \quad (2)$$

where ρ is the air density (kg/m^3); μ is the dynamic viscosity coefficient (Pa·s); ν is the kinematic viscosity coefficient (m^2/s); x_i and x_j are the space coordinate components, i, j=1, 2, 3; u_i is the time-averaged air velocity component (m/s); t is the time; G_k is the turbulence kinetic energy generation term induced by the mean velocity gradient; S is the strain rate; μ_t is the turbulence viscosity coefficient, and $\mu_t=\rho C_\mu k^2/\varepsilon$, where C_μ and C_1 are the modeling coefficients, and the calculation equations are given in previous studies (Tavoularis and Corrsin, 1981; Shih et al., 1995b). The modeling constants σ_k, σ_ε, and C_2 are 1.0, 1.2, and 1.9, respectively (Mohamed and Larue, 1990; Shih et al., 1995a). The non-equilibrium wall function is selected for the treatment of the near-wall region, and the finite-volume method is used to discretize the control equations. The steady-state iterative solution of the velocity and pressure fields is solved using the semi-implicit method for pressure-linked equations (SIMPLE) algorithm.

2.2 Physical model and boundary conditions

Integrated computer engineering and manufacturing (ICEM) 19.2 is used to establish a full-scale model of a parallel confluence tunnel with a rectangular cross-section, and Fluent 2019R1 is used to conduct numerical calculations. The corresponding cross-sectional dimensions of the mainline and the ramp are 13 m×5 m and 9.5 m×5 m, respectively; the length of the parallel section is 70 m, with cross-sectional dimensions of 22.5 m×5 m; the length of the gradual transition section is 40 m, with a tapering angle α of 9.46°; the confluence angles of the tunnel are considered with three cases of 5°, 10°, and 15°.

A more regular hexahedral mesh is used to discretize the computational domain, so as to guarantee the calculation accuracy and improve the calculation efficiency. The area near the tunnel intersection surface (within 10 times the hydraulic diameter of the section from the intersection surface) (Shi et al., 2013) is locally refined as shown in Fig. 2. In addition, a boundary layer mesh is set near the tunnel wall. The non-equilibrium wall function requires that the dimensionless distance parameter y^+ of the wall is distributed between 30 and 300 (Qin et al., 2006), and the distance of the first grid node of the boundary layer from the wall is back-projected according to y^+, which is constantly corrected through computational simulation. It is ultimately determined that when the thickness of the first grid layer is 0.015 m, we can ensure that y^+ is between 32 and 291 for all computational conditions.

The tunnel wall and road surface are set as no-penetration and non-slip boundaries. The mainline and ramp entrances before the confluence are set to Dirichlet boundary conditions given uniform wind speeds, and the mainline exits after the confluence are set to Neumann boundary conditions with free outflow.

2.3 Grid independence study

Grid density has a significant influence on the accuracy of numerical simulations. A sparse grid leads to substantial discretization errors, whereas a dense grid not only increases rounding errors but also boosts the computational load. Four gridding schemes are given in Table 1, and Fig. 3 shows the average flow velocity (u) profile of the mainline tunnel cross-section after confluence at 5D (D represents the hydraulic diameter) downstream of the intersection surface when the confluence angle θ is 10° and the confluence ratio q is 0.9 (q represents the ratio of the volumetric flow rate of air on the ramp to that on the mainline after the confluence) under each gridding scheme. Y represents the width of the cross-section. It is clear that the grid size has a large impact on the velocity distribution, and when the number of grids reaches 2.05×10^6, the velocity distribution will no longer change significantly. Furthermore, the grid size of scheme 2 meets the requirements of grid independence, so we adopt this scheme as the basis for setting the grid profiles for other working conditions.

2.4 Model validation

The mathematical model is validated using the test results of the parallel bifurcated tunnel ventilation scale model from Zhejiang University with a 1/20 geometric scale (Fig. 4). The scale model is constructed based on similarity theory, with velocity scale λ_u and pressure scale λ_p equaling 1, and length scale λ_l and time scale λ_t equaling 20, which can simultaneously satisfy the Eu, Re, and Sr similarity criteria when the experimental air velocity is greater than or equal to 2.5 m/s.

The main body of the model consists of five parts: the mainline before confluence, the mainline after confluence, the confluence ramp, the parallel section, and the gradual transition section. These segments measure 10.46 m, 19.00 m, 9.23 m, 3.50 m (L_{para}), and 2.00 m (L_{grad}) in length, respectively. Each section has a rectangular cross-section, with dimensions for the

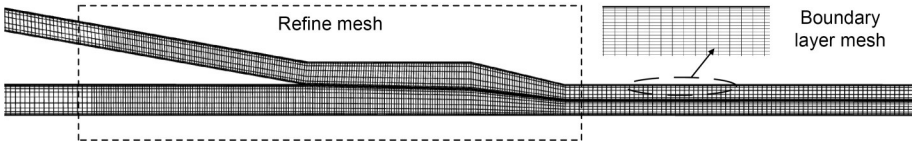

Fig. 2 Schematic diagram of the grid division of the parallel bifurcated tunnel

Table 1 Grid independence test cases

Gridding scheme	Grid size				Total grid number
	Length (m)		Width (m)	Height (m)	
	Coarse grid	Refine grid			
1	2.0	1.0	0.6	0.30	2.10×10^5
2	1.0	0.5	0.3	0.15	2.05×10^6
3	0.8	0.4	0.2	0.10	5.74×10^6
4	0.6	0.3	0.2	0.10	7.64×10^6

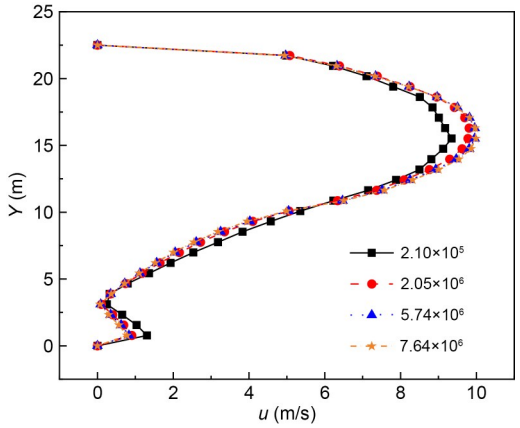

Fig. 3 Velocity profiles for different grid schemes

mainline, ramp, and parallel section being 0.65 m× 0.25 m, 0.475 m×0.25 m, and 1.12 m×0.25 m, respectively. Additionally, the confluence angle θ is adjustable from 0° to 30°. To simulate a jet fan, an inverter high-pressure fan connects through a diversion pipe to a nozzle, which comprises a pumping pipe and a jet pipe, capable of achieving a maximum jet velocity of 50 m/s. For data acquisition, the SENTRY ST732 hot-wire anemometer, with a measurement range of 0–40 m/s and an accuracy of 0.03 m/s, along with the Alpha Model 166 micro-pressure differential meter, which has a measurement range of 0–50 Pa with an accuracy of 0.25% full scale (FS), was employed to collect air velocity and pressure data at each measurement point.

For the specific experiments, fan #3, positioned in the mainline tunnel post-confluence, was activated to ensure that airflow within the model tunnel reached the self-modeling zone. Concurrently, the wind speeds of fans #1 and #2, located in the mainline tunnel and ramp prior to the confluence, respectively, were adjusted to modify the confluence ratio q from 0.1 to 0.9 To confirm that the flow at the measurement section was fully developed turbulence, the air velocity and pressure measurement locations were strategically placed at least 10 times the hydraulic diameter away from the tunnel's bifurcation point. For areas with fully developed turbulent flow, the static pressure is uniformly distributed across the section, and the average flow velocity u is linearly proportional to the maximum flow velocity u_{max}, expressed as $u=a_i u_{max}$ (i=1, 2, 3), where a_i is the correction coefficient. Accordingly, the air velocity measurement point was positioned at the center of the section, while the pressure measurement point was set at d=0.1 m, as illustrated in Fig. 5. The correction coefficients a_1, a_2, and a_3 for sections 1-1, 2-2, and 3-3 were determined to be 0.81, 0.80, and 0.81, respectively.

The air velocity and pressure data were measured at the steady stage, i.e., both air velocity and pressure

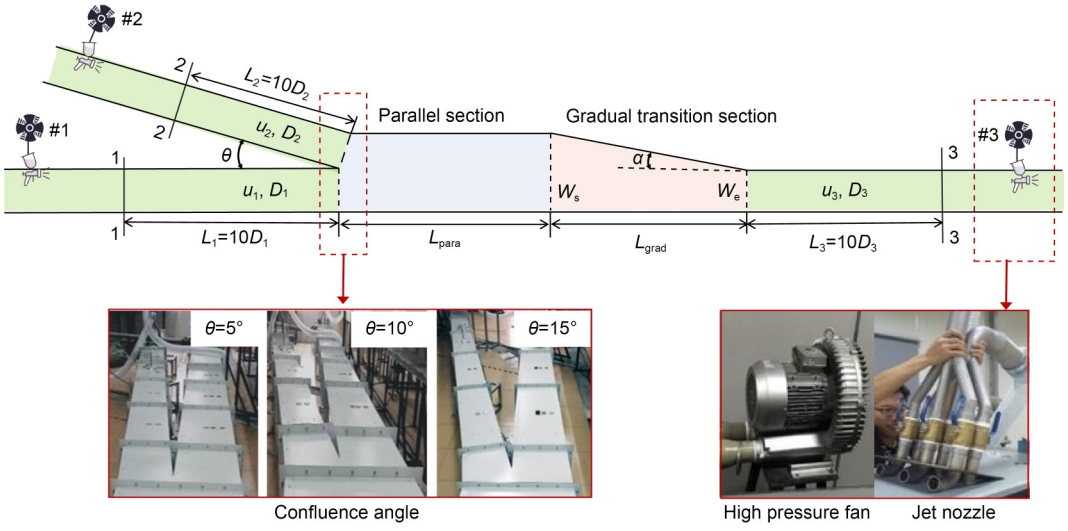

Fig. 4 Ventilation scale model tunnel experimental platform for the parallel bifurcation tunnel. L_1 and L_2 represent the lengths of the sections 1–1 and 2–2 from the intersection section, respectively; L_3 represents the distance from the end of the gradual transition section to section 3–3; D_1, D_2, and D_3 are the hydraulic diameters of the mainline before confluence, confluence ramp, and mainline after confluence, respectively; u_1, u_2, and u_3 are the air velocities of the mainline before confluence, confluence ramp, and mainline after confluence, respectively; W_s and W_e are the widths at both ends of the gradual transition section

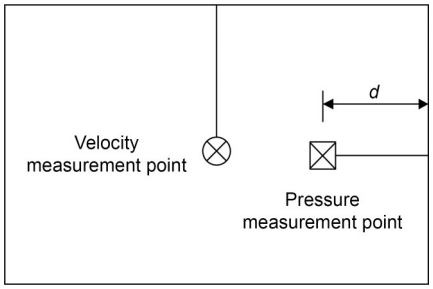

Fig. 5 Velocity and pressure measurement points on the section

did not change significantly with time. The averaging time was designed to be long enough to reduce the uncertainty (e.g., around 1 min in this study). The standard errors of air velocity and pressure data measured in all experimental conditions did not exceed 0.07. Taking the measurement of velocity and pressure values on the 2-2 cross-section of the ramp at θ=15° as an example, the fluctuations during the measurement were presented and plotted with an error bar and violin plot in the revision, as shown in Fig. 6.

Utilizing the experimental data, the confluence loss coefficients for the mainline (K_{13}) and ramp (K_{23}) of the parallel bifurcated tunnel can be determined using Eqs. (3) and (4) (Bassett et al., 2001):

$$K_{13}=\frac{\left(p_1+\frac{1}{2}\rho u_1^2\right)-\left(p_3+\frac{1}{2}\rho u_3^2\right)-\Delta p_1-\Delta p_3}{\frac{1}{2}\rho u_3^2}, \quad (3)$$

$$K_{23}=\frac{\left(p_2+\frac{1}{2}\rho u_2^2\right)-\left(p_3+\frac{1}{2}\rho u_3^2\right)-\Delta p_2-\Delta p_3}{\frac{1}{2}\rho u_3^2}, \quad (4)$$

where subscripts 1, 2, and 3 represent the measurement points located in the mainline before confluence, ramp, and mainline after confluence, respectively. Δp_i

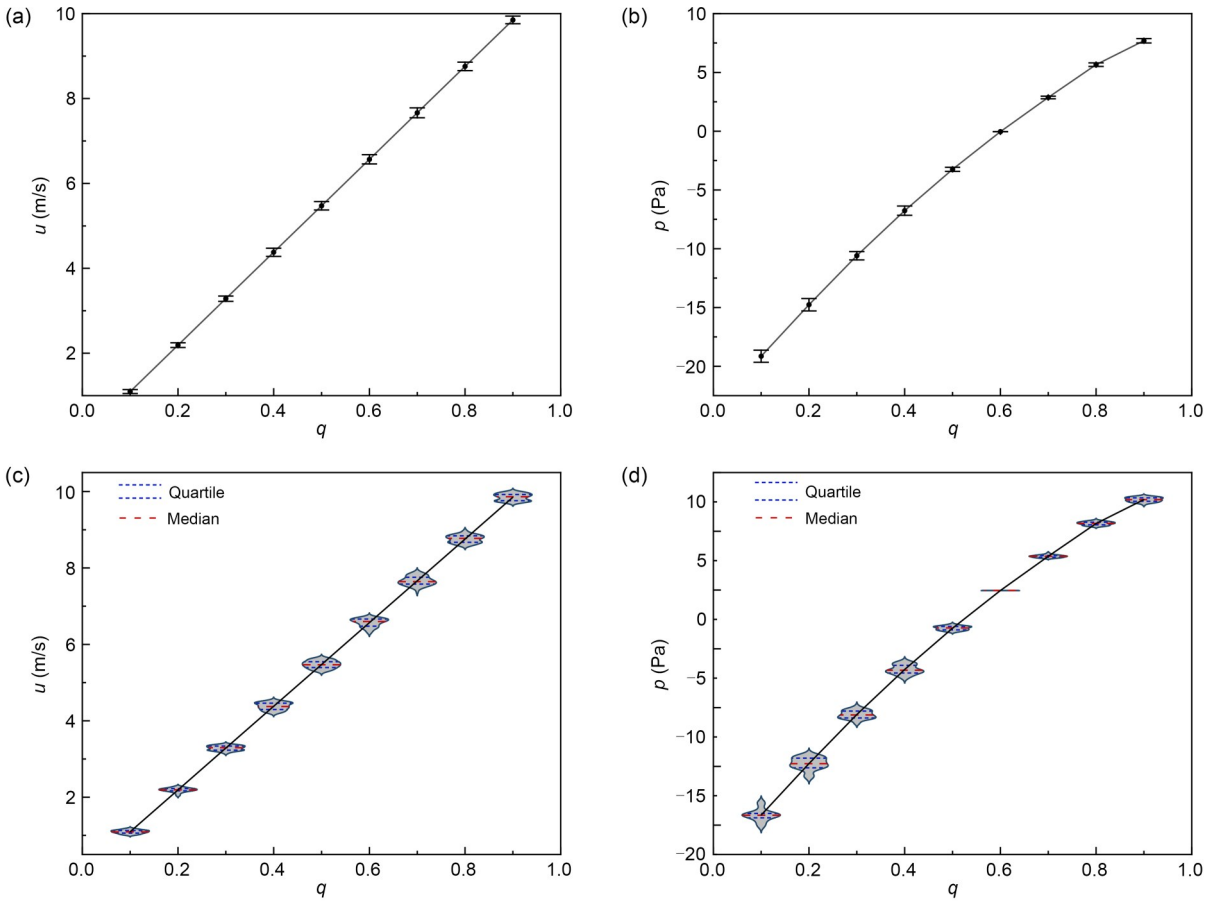

Fig. 6 Air velocity and pressure in 2–2 cross-section of the confluence ramp under different q values: (a) air velocity, error bar; (b) static pressure, error bar; (c) air velocity, violin plot; (d) static pressure, violin plot. Error bars represent the standard deviation. p represents the surface-averaged weighted static pressure at the measurement point (Pa)

represents the frictional loss pressure drop across a tunnel section of length L_i (Pa), which is calculated:

$$\Delta p_i = \frac{\lambda_i L_i \rho u_i^2}{2D_i},\ i = 1,\ 2,\ 3, \tag{5}$$

where λ_i denotes the coefficient of frictional loss for the section containing the measurement point.

Fig. 7 compares the numerical simulation data with the test results for the loss coefficients for a parallel confluence section at θ=15°. The mainline confluence loss coefficient K_{13} decreases as q increases, while the ramp confluence loss coefficient K_{23} increases with q. The simulation results align well with the test data, showing a maximum deviation of less than 10%. This demonstrates that the numerical model effectively captures the flow field characteristics and loss variations in the parallel confluence section.

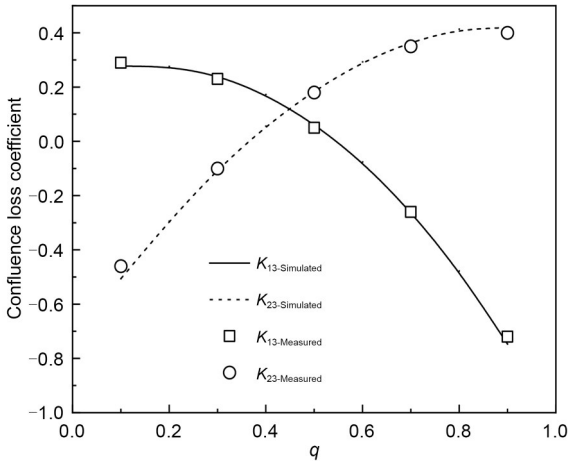

Fig. 7 Comparison of simulated data and experimental results of loss coefficients for the parallel confluence section

3 Results and discussion

3.1 Effect of the confluence ratio q

Air from the mainline and ramp converges at the bifurcation, flows through the parallel section and gradual transition section, and ultimately merges into the mainline tunnel. Fig. 8 depicts the flow field structure of the parallel confluence section at various confluence ratios q when the confluence angle θ is 15°. Fig. 9 illustrates the variations in the mainline confluence loss coefficient K_{13}, ramp confluence loss coefficient K_{23}, and the total tunnel confluence loss coefficient K (K= $|K_{13}|$ + $|K_{23}|$) under corresponding conditions. The loss coefficient data presented in this section are all derived from numerical simulations.

Figs. 8 and 9 demonstrate that at q=0.1, the airflow ratio Q=9.00 between the mainline and the ramp prior to confluence significantly exceeds their cross-sectional area ratio φ=1.37. At this point, the airflow velocity in the mainline substantially surpasses the velocity in the ramp. As these two airflows with different velocities meet and interact in the parallel section, they form a cross-section with discontinuous velocities. The faster airflow from the mainline strongly entrains the slower airflow from the ramp, causing a marked flow separation at the junction between the parallel section and the gradual transition section. This results in a high total loss coefficient K at the tunnel confluence. During this entrainment, the airflow velocity in the mainline first decreases and then increases, prompting the mainline flow to initially diverge towards the ramp and then contract. This behavior leads to a positive mainline confluence loss coefficient K_{13}. Conversely, the ramp's airflow experiences a significant increase in velocity and pressure due to the entrainment by the high-velocity

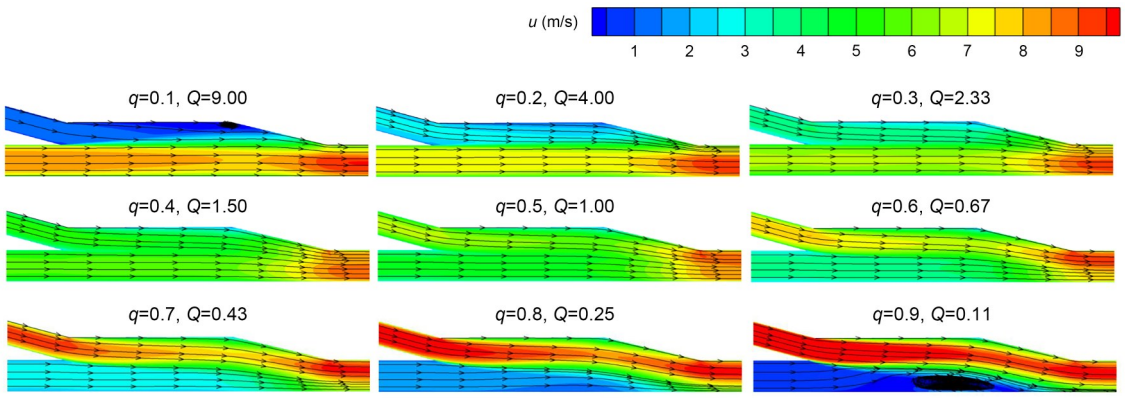

Fig. 8 Flow field structure of the parallel confluence section at θ=15°

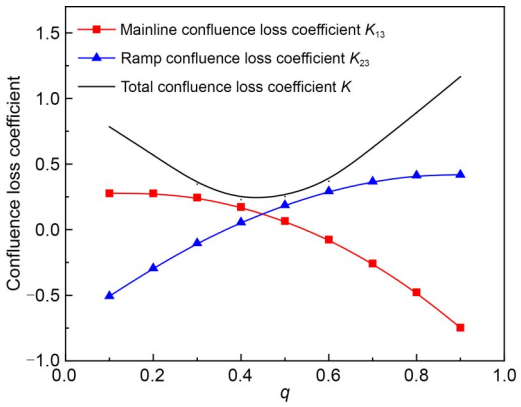

Fig. 9 Variations of the loss coefficients in the parallel confluence section

mainline airflow, resulting in a negative ramp confluence loss coefficient K_{23}.

With the increase of q, the airflow converging into the mainline from the ramp increases, making Q gradually approach φ. Consequently, the velocity gradient in the cross-section of the parallel section decreases, resulting in a more uniform airflow. This diminishing velocity difference weakens the entrainment effect between the two airstreams and leads to a gradual disappearance of flow separation and a reduction in total loss coefficient K at the tunnel confluence. During this process, there is a decrease in mainline flow line dispersion bending, leading to a reduced value of K_{13} ($|K_{13}|$ decreases, approaching 0). Conversely, due to the weakened jet entrainment and pressurization effects on ramp airflow, K_{23} gradually increases ($|K_{23}|$ approaches 0). When Q is close to φ (such as q=0.4 or q=0.5 conditions), the flow tends to be smooth, the jet pressurization effect basically disappears, and the loss coefficients $|K_{13}|$ and $|K_{23}|$ tend to be extremely small values.

As q increases further (e.g., $q\geqslant0.6$), more air enters the mainline tunnel from the ramp, resulting in Q being less than φ. At this point, the airflow velocity in the mainline before the tunnel confluence becomes lower than that in the ramp, disrupting the uniform flow in the tunnel confluence section of the tunnel and gradually increasing the velocity gradient across the section. When q reaches 0.9, significant flow separation occurs near the mainline side of the confluence section, leading to a rise in the total loss coefficient K. During this process, the low-speed airflow in the mainline before the confluence experiences an increase in velocity and pressure due to the jet entrainment effect of the high-speed ramp airflow, causing K_{13} to become negative. As q increases, the difference in airflow velocity between the mainline and the ramp grows, intensifying the jet entrainment and pressurization effects and reducing K_{13} ($|K_{13}|$ increases). The ramp's airflow velocity decreases and then increases as it converges into the mainline, causing the ramp flow line to initially diverge and bend towards the mainline before contracting, resulting in local losses. Consequently, K_{23} becomes positive, and as q increases, the degree of flow line bending and K_{23} both increase ($|K_{23}|$ increases).

These results indicate that in the parallel confluence section, a mismatch between the airflow ratio Q and the cross-sectional area ratio φ of the mainline and ramp before the confluence increases the velocity gradient across the confluence section. This mismatch enhances the jet entrainment effect, intensifies streamline bending and flow separation, and consequently results in a higher total loss coefficient K for the tunnel confluence, as well as increased loss coefficients $|K_{13}|$ and $|K_{23}|$ for the mainline and ramp confluence, respectively. When $Q>\varphi$, K_{13} is primarily influenced by the degree of streamline divergence and bending, while K_{23} is mainly affected by the jet entrainment and pressurization effects. Conversely, when $Q<\varphi$, the primary factors influencing K_{13} and K_{23} are reversed.

3.2 Effect of the confluence angle θ

Fig. 10 shows the flow field structure of the parallel confluence section for different θ values. Fig. 11 presents the variation of the total loss coefficient K of tunnel confluence for different θ values, while Fig. 12 shows the loss coefficients K_{13} and K_{23} of the mainline and ramp confluence with q for different θ values. The loss coefficient data presented in this section are all derived from numerical simulations.

As shown in Fig. 10a, when q is small, most of the air flows into the confluence section from the mainline. The high-speed airflow on the mainline entrains the low-speed airflow on the ramp, leading to noticeable flow separation in the confluence section near the ramp side. The air streamline on the mainline initially diverges and then contracts. Comparing the flow field structures for different θ values, it is evident that the extent of flow separation caused by the entrainment effect and the degree of streamline curvature are almost

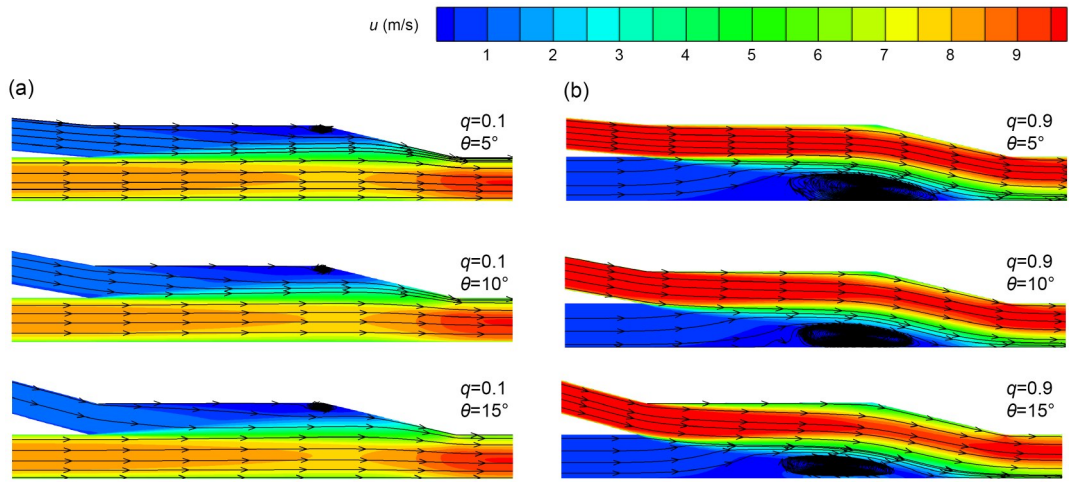

Fig. 10 Flow field structures of the parallel confluence section for different θ values: (a) q=0.1; (b) q=0.9

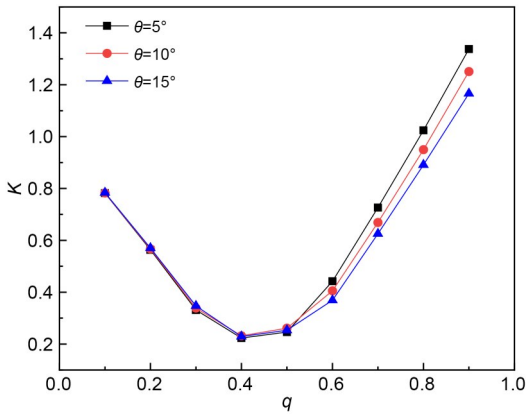

Fig. 11 Total loss coefficients in the parallel confluence section for different θ values

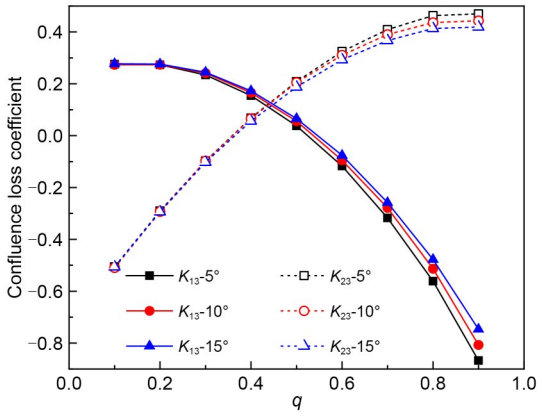

Fig. 12 Loss coefficients of the mainline and ramp in the parallel confluence section for different θ values

unaffected by θ. Therefore, when q is small, the influence of θ on the total loss coefficient K of the parallel confluence section, as well as the confluence loss coefficients K_{13} and K_{23} of the mainline and ramp, is minimal. This is illustrated in Figs. 11 and 12.

Fig. 10b shows that when q=0.9, most of the air flows into the confluence section from the ramp. The high-speed airflow on the ramp entrains the low-speed airflow on the mainline, causing significant flow separation on the mainline side of the confluence section, while the air streamlines on the ramp undergo severe bending. At this stage, K_{13} is primarily influenced by the jet entrainment and pressurization, while K_{23} is mainly affected by the degree of streamline curvature. Comparing the flow field structures for different θ values, we observe that larger θ results in a smaller range of flow separation on the mainline side and weaker curvature of the ramp streamline. Consequently, the total loss coefficient K of the parallel confluence section, as well as the confluence loss coefficients $|K_{13}|$ and $|K_{23}|$ of the mainline and ramp, is reduced, as shown in Figs. 11 and 12.

3.3 Predictive model of loss coefficients in the parallel confluence section

Bassett et al. (2001) derived a formula for the local loss coefficient of a three-way pipe confluence, applicable for any confluence angle θ and cross-sectional area ratio φ, based on the continuity equation, momentum conservation, and Bernoulli's equation, as shown in Eqs. (6) and (7). The accuracy of Bassett's formula in predicting local loss coefficients for 45°–120° confluence bifurcations has been widely validated. Therefore, in this study, Bassett's formula is used to predict the loss coefficients of the parallel-type confluence

section and is compared with the experimental data, as shown in Fig. 13.

$$K_{13\text{-Bassett}}=\frac{2\varphi\left[1-(1-q)^2-q^2\varphi\cos(0.75\theta)\right]}{\varphi+\frac{1}{2}\cos(0.75\theta)}+(1-q)^2-1, \tag{6}$$

$$K_{23\text{-Bassett}}=\frac{2\varphi\left[1-(1-q)^2-q^2\varphi\cos(0.75\theta)\right]}{\varphi+\frac{1}{2}\cos(0.75\theta)}+q^2\varphi^2-1, \tag{7}$$

where $K_{13\text{-Bassett}}$ and $K_{23\text{-Bassett}}$ are mainline loss coefficients and ramp loss coefficients of the parallel-type confluence section, respectively.

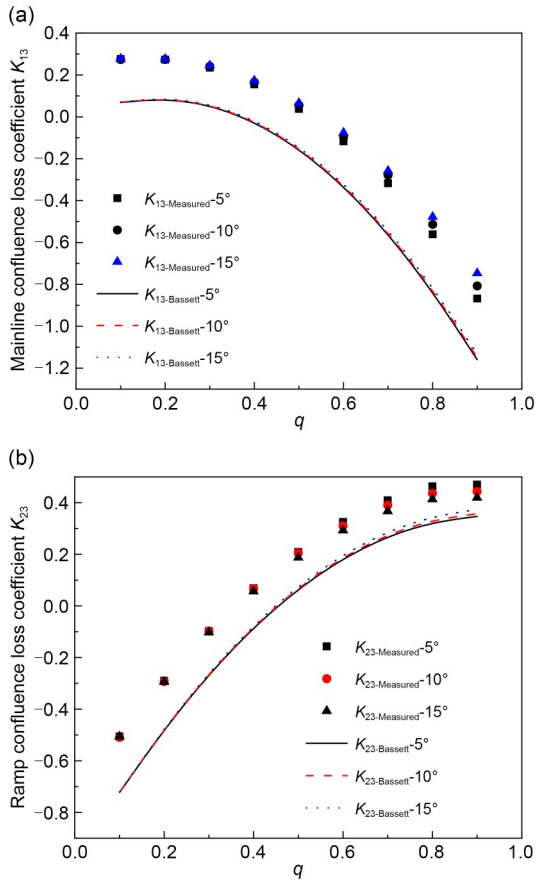

Fig. 13 Comparison of calculation results from Bassett's formula and the test results: (a) mainline confluence loss coefficient K_{13}; (b) ramp loss confluence coefficient K_{23}

For the parallel confluence mainline and ramp loss coefficients, the predicted values from Bassett's formula are generally low. The deviation between the predicted and experimental values of the mainline confluence coefficient K_{13} increases with q, while the deviation between the predicted and experimental values of the ramp loss coefficient K_{23} decreases with q. This discrepancy arises because Bassett's formula is derived from a bifurcated tee pipe model, where the main pipe's cross-sectional area remains unchanged before and after the confluence. For parallel confluence bifurcations, the cross-sectional area of the mainline before and after the confluence is inconsistent, and the air of the ramps and the mainline will generate additional "sudden expansion-gradual contraction" losses when flowing through the parallel section and the gradual change section. This is the primary reason why the predicted values of $|K_{13}|$ and $|K_{23}|$ from Bassett's equations are significantly lower.

Additionally, the predicted $|K_{13}|$ from Bassett's formula is almost unaffected by θ at larger q, while the predicted $|K_{23}|$ increases slightly with θ, which contradicts the experimental results. Bassett assumed that the fluid flow direction in the branch was not exactly parallel to the axial direction of the branch and thus corrected the confluence angle of the ramp inflow to the mainline based on Hager's assumption (Hager, 1984). However, Hager's assumption is based on the confluence flow phenomenon in branch pipes with confluence angles greater than 45°. Therefore, Bassett's formula is not suitable for predicting loss coefficients in parallel-type confluence sections with small confluence angles (5°–15°).

Considering the change in the main control factors of the loss coefficient with varying confluence ratio q, the 0.75θ in Eqs. (6) and (7) has been revised to θ_{13} and θ_{23}, respectively. Additionally, by incorporating the "sudden expansion-gradual contraction" loss $\zeta(\xi_{\text{para}}+\xi_{\text{grad}})$ to account for the influence of parallel confluence loss, the parallel confluence mainline and ramp loss coefficients can be expressed as follows:

$$\begin{aligned}K_{13\text{-Formula}}&=K'_{13\text{-Bassett}}+\zeta(\xi_{\text{para}}+\xi_{\text{grad}}),\\ K_{23\text{-Formula}}&=K'_{23\text{-Bassett}}+\zeta(\xi_{\text{para}}+\xi_{\text{grad}}),\end{aligned} \tag{8}$$

where $K'_{13\text{-Bassett}}$ and $K'_{23\text{-Bassett}}$ are the parts corresponding to the bifurcation loss in the confluence loss coefficients of the mainline and the ramp after correcting the confluence angle; ξ_{para} and ξ_{grad} are the loss coefficients of the parallel section and the gradual transition section, respectively. The correction coefficient ζ

accounts for the mutual influence of losses when the bifurcation segment connects with the parallel section and transition section. The expressions for $K'_{13\text{-Bassett}}$, $K'_{23\text{-Bassett}}$, ξ_{para}, and ξ_{grad} are as follows:

$$K'_{13\text{-Bassett}}=\frac{2\varphi\left[1-(1-q)^2-q^2\varphi\cos\theta_{13}\right]}{\varphi+\frac{1}{2}\cos\theta_{13}}+(1-q)^2-1,$$

$$K'_{23\text{-Bassett}}=\frac{2\varphi\left[1-(1-q)^2-q^2\varphi\cos\theta_{23}\right]}{\varphi+\frac{1}{2}\cos\theta_{23}}+q^2\varphi^2-1,$$

$$\xi_{\text{para}}=\lambda\frac{L_{\text{para}}}{D_{\text{para}}}\left(\frac{W_{\text{s}}}{W_{\text{e}}}\right)^2,$$

$$\xi_{\text{grad}}=\frac{\lambda W_{\text{e}}^2}{2H\tan\alpha}\left[H\left(\frac{1}{2W_{\text{e}}^2}-\frac{1}{2W_{\text{s}}^2}\right)+\left(\frac{1}{W_{\text{e}}}-\frac{1}{W_{\text{s}}}\right)\right], \tag{9}$$

where λ is the coefficient of frictional loss; D_{para} is the hydraulic diameter of the parallel section; H is the height of the tunnel (m). Based on the test results and simulation data, the fitted values are ζ=0.6, θ_{13}=17.31+4.535q−1.168+θ, and θ_{23}=41.32q−0.498−θ−23.62, with goodness-of-fit values for $K_{13\text{-Formula}}$ and $K_{23\text{-Formula}}$ of 0.97 and 0.99, respectively.

Fig. 14 compares Bassett's formula, the model proposed in this paper, and the test results. The figure shows that the predictions from our proposed model align well with the test values, significantly improving the accuracy compared to Bassett's formula. Additionally, this model accurately reflects the trend that when the q is large, $|K_{13}|$ and $|K_{23}|$ decrease with increasing θ, thus addressing the discrepancy where Bassett's formula predicts the opposite trend from the experimental results.

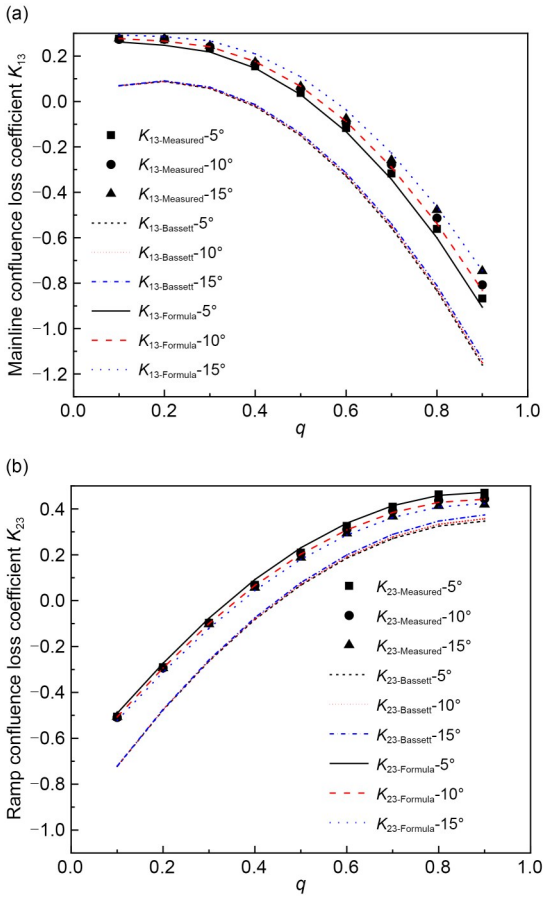

Fig. 14 Comparison of the proposed formula, Bassett's formula calculation results, and test results: (a) mainline confluence loss coefficient K_{13}; (b) ramp confluence loss coefficient K_{23}

4 Conclusions

This work presented a numerical and experimental investigation of the flow characteristics and loss coefficients induced by the bifurcated structure of parallel confluence sections in tunnels, considering the effects of the confluence ratio q and confluence angle θ. It was found that when air flows through the parallel confluence section, two airflows with unequal velocities collide in the parallel section, forming a section with discontinuous velocity and generating an entrainment effect. For small q, the high-speed mainline airflow entrains the low-speed ramp airflow, causing flow separation at the upper part of the connection between the parallel acceleration section and the gradient section. For large q, the high-speed ramp airflow entrains the low-speed mainline airflow, causing flow separation near the mainline side of the confluence section.

Losses in the parallel confluence section are primarily due to changes in flow velocity gradient, streamline bending, and flow separation caused by the sudden changes in flow field structure and jet entrainment effect. As q changes, the mismatch between the volumetric flow rate ratio Q and the cross-section area ratio φ between the mainline tunnel and the ramp before confluence increases the velocity gradient in the cross-section of the confluence section, enhances the jet entrainment effect, and intensifies streamline bending

and flow separation, resulting in larger local loss coefficients $|K_{13}|$ and $|K_{23}|$.

For small q, the flow separation range and streamline bending caused by the entrainment effect are almost unaffected by θ, resulting in K_{13} and K_{23} remaining relatively constant with θ. For large q, as θ increases, the flow separation range on the mainline side decreases, and the degree of streamline bending in the ramp weakens, leading to a reduction in the loss coefficients $|K_{13}|$ and $|K_{23}|$.

A semi-empirical formula was proposed which can accurately predict the loss coefficients for 5°–15° parallel confluence tunnels. This formula incorporates the local loss of the flow field due to "sudden expansion-gradual contraction" effects and corrects the angle of the flow line, addressing the shortcomings in traditional ventilation design theory for bifurcated tunnels.

By decoupling the effects of the confluence ratio q and confluence angle θ on the complex flow field, this work provides a deeper understanding of the aerodynamic behaviour and loss mechanisms in bifurcated tunnels. Accordingly, it offers a scientific basis for optimising the design of tunnel ventilation systems and environment control technology in tunnel-like underground infrastructure.

Acknowledgments

This work is supported by the National Natural Science Foundation of China (Nos. 52408439 and 52478422), the Natural Science Basic Research Program of Shaanxi (No. 2023-JC-YB-378), China, the Young Talent Fund of Xi'an Association for Science and Technology (No. 0959202513050), China, the Fundamental Research Funds for the Zhejiang Provincial Universities (No. 226-2024-00099), China, the Postdoctoral Fellowship Program of China Postdoctoral Science Foundation (No. GZC20241518), and the Xi'an Shiyou University Graduate Student Innovation Fund Program (No. YCX2512041), China.

Author contributions

Xin ZHANG, Tianhang ZHANG, and Ke WU designed the research. Xin ZHANG and Hao HE wrote the first draft of the manuscript. Hao HE and Xiaofeng CHEN processed the corresponding data. Xiaofeng CHEN and Kai ZHU carried out the scale model experiment. Yachao LI and Yuehui WANG investigated and summarized the types of tunnel bifurcations and related engineering parameters. Tianhang ZHANG and Ke WU revised and edited the final version.

Conflict of interest

The authors declare that they have no conflict of interest.

References

Abou-Haidar NI, Dixon SL, 1992. Pressure losses in combining subsonic flows through branched ducts. *Journal of Turbomachinery*, 114(1):264-270. https://doi.org/10.1115/1.2927994

Bassett MD, Winterbone DE, Pearson RJ, 2001. Calculation of steady flow pressure loss coefficients for pipe junctions. *Proceedings of the Institution of Mechanical Engineers, Part C: Journal of Mechanical Engineering Science*, 215(8):861-881. https://doi.org/10.1177/095440620121500801

Blaisdell FW, Manson PW, 1963. Loss of Energy at Sharp-Edged Pipe Junctions in Water Conveyance Systems. Technical Bulletin 1283, US Department of Agriculture, USA.

Chen T, Zhou D, Lu ZJ, et al., 2021. Study of the applicability and optimal arrangement of alternative jet fans in curved road tunnel complexes. *Tunnelling and Underground Space Technology*, 108:103721. https://doi.org/10.1016/j.tust.2020.103721

Chen ZE, Chen XF, Kong XM, et al., 2024. Study on the flow characteristics and local loss characteristics of the confluence segment of bifurcate tunnel. *Modern Tunnelling Technology*, 61(3):53-60 (in Chinese). https://doi.org/10.13807/j.cnki.mtt.2024.03.007

Gao ZH, Liu MG, Zhao PJ, et al., 2024. Influence of tunnel slope on the one-dimensional spread of smoke transportation and temperature distribution in tunnel fires. *Tunnelling and Underground Space Technology*, 146:105650. https://doi.org/10.1016/j.tust.2024.105650

Gardel AE, 1957. Les pertes de charge dans les ecoulements au travers de branchments en te. *Bulletin Technique de la Suisse Romande*, 83(9):123-130 (in French).

Hager WH, 1984. An approximate treatment of flow in branches and bends. *Proceedings of the Institution of Mechanical Engineers, Part C: Journal of Mechanical Engineering Science*, 198(1):63-69. https://doi.org/10.1243/PIME_PROC_1984_198_088_02

Itō H, Imai K, 1973. Energy losses at 90° pipe junctions. *Journal of the Hydraulics Division*, 99(9):1353-1368. https://doi.org/10.1061/JYCEAJ.0003733

Jafari S, Farhanieh B, Afshin H, 2023. Numerical investigation of critical velocity in curved tunnels: parametric study and establishment of new model. *Tunnelling and Underground Space Technology*, 135:105021. https://doi.org/10.1016/j.tust.2023.105021

Król A, Król M, 2021. Numerical investigation on fire accident and evacuation in a urban tunnel for different traffic conditions. *Tunnelling and Underground Space Technology*, 109:103751. https://doi.org/10.1016/j.tust.2020.103751

Li L, Li YL, Huang JT, et al., 2001. Numerical simulation and experimental study on water flow in Y-type tube. *Journal of Hydraulic Engineering*, (3):49-53 (in Chinese). https://doi.org/10.3321/j.issn:0559-9350.2001.03.010

Liang CJY, Nan S, Shao XL, et al., 2021. Calculation method for air resistance coefficient of vehicles in tunnel with different traffic conditions. *Journal of Building Engineering*, 44:102971.

https://doi.org/10.1016/j.jobe.2021.102971

Liu F, Yin C, Chen JZ, et al., 2020. Numerical simulation study on the influence of intersection angle of confluence section on ventilation characteristics of freeway tunnel. *Modern Tunnelling Technology*, 57(S1):645-650 (in Chinese). https://doi.org/10.13807/j.cnki.mtt.2020.S1.086

Miller DS, 1971. Internal Flow: a Guide to Losses in Pipe and Duct Systems. British Hydromechanics Research Association, Cranfield, UK, p.303-360.

Mohamed MS, Larue JC, 1990. The decay power law in grid-generated turbulence. *Journal of Fluid Mechanics*, 219: 195-214. https://doi.org/10.1017/S0022112090002919

Oka K, Nozaki T, Ito H, 1996. Energy losses due to combination of flow at tees. *JSME International Journal Series B Fluids and Thermal Engineering*, 39(3):489-498. https://doi.org/10.1299/jsmeb.39.489

Qin WJ, Hu CG, Guo LP, et al., 2006. Effect of near-wall grid size on turbulent flow solutions. *Transactions of Beijing Institute of Technology*, 26(5):388-392 (in Chinese). https://doi.org/10.3969/j.issn.1001-0645.2006.05.003

Shi X, Lü HX, Zhu DL, et al., 2013. Flow resistance and characteristics of PVC tee pipes. *Transactions of the Chinese Society for Agricultural Machinery*, 44(1):73-79 (in Chinese). https://doi.org/10.6041/j.issn.1000-1298.2013.01.015

Shih TH, Liou WW, Shabbir A, et al., 1995a. A new $k-\epsilon$ eddy viscosity model for high Reynolds number turbulent flows. *Computers & Fluids*, 24(3):227-238. https://doi.org/10.1016/0045-7930(94)00032-T

Shih TH, Zhu J, Lumley JL, 1995b. A new Reynolds stress algebraic equation model. *Computer Methods in Applied Mechanics and Engineering*, 125(1-4):287-302. https://doi.org/10.1016/0045-7825(95)00796-4

Tavoularis S, Corrsin S, 1981. Experiments in nearly homogeneous turbulent shear flow with a uniform mean temperature gradient. Part 2. The fine structure. *Journal of Fluid Mechanics*, 104:349-367. https://doi.org/10.1017/S0022112081002942

Wang MN, Deng T, Yu L, 2024. Development and prospects of operation and disaster prevention ventilation technology in China's traffic tunnels. *Modern Tunnelling Technology*, 61(2):152-166 (in Chinese). https://doi.org/10.13807/j.cnki.mtt.2024.02.014

Xu FQ, Du ZG, Chen C, 2022. Distribution and development characteristics of urban road tunnels in China. *Modern Tunnelling Technology*, 59(6):35-41 (in Chinese). https://doi.org/10.13807/j.cnki.mtt.2022.06.004

Zhang X, Zhang TT, Huang ZY, et al., 2018. Local loss and flow characteristic of dividing flow in bifurcated tunnel. *Journal of Zhejiang University (Engineering Science)*, 52(3):440-445 (in Chinese). https://doi.org/10.3785/j.issn.1008-973X.2018.03.004

Zhang X, Zhang TH, Hou YG, et al., 2019. Local loss model of dividing flow in a bifurcate tunnel with a small angle. *Journal of Zhejiang University-SCIENCE A (Applied Physics & Engineering)*, 20(1):21-35. https://doi.org/10.1631/jzus.A1800298

Zhang X, Guo S, Dang XY, et al., 2024. Experimental investigation on the influence of portal-blocking speed on fire behaviors in tunnel structure. *Case Studies in Thermal Engineering*, 53:103811. https://doi.org/10.1016/j.csite.2023.103811

Zhu K, Hu HP, Zhang X, et al., 2024. Influence of tunnel bifurcation form on the local ventilation resistance characteristics of dividing flow. *Journal of China University of Metrology*, 35(2):197-202 (in Chinese). https://doi.org/10.3969/j.issn.2096-2835.2024.02.002